Arsenic stress triggers active exudation of arsenic-phytochelatin complexes from *Lupinus albus* roots

Adrien Frémont[1,2], Eszter Sas[1], Mathieu Sarrazin[3], Jacques Brisson[1], Frédéric Emmanuel Pitre[1,4], Nicholas James Beresford Brereton[5]

[1] Institut de recherche en biologie végétale, Université de Montréal, 4101 Sherbrooke Est, Montréal, QC H1X 2B2, Canada

[2] Environmental Genomics and Systems Biology, Lawrence Berkeley National Laboratory, Berkeley, CA, USA

[3] Collège de Maisonneuve CÉPROCQ, 6220 Sherbrooke Est, Montréal, Québec, Canada

[4] Montreal Botanical Garden, 4101 Sherbrooke Est, Montreal, Québec, Canada

[5] School of Biology and Environmental Science, University College Dublin, Belfield, Dublin 4, Ireland

Adrien Frémont: afremont@lbl.gov

Eszter Sas: eszter.sas@umontreal.ca

Mathieu Sarrazin: msarrazin@cmaisonneuve.qc.ca

Jacques Brisson: jacques.brisson@umontreal.ca

Frédéric Emmanuel Pitre: frederic.pitre@umontreal.ca

Nicholas James Beresford Brereton: nicholas.brereton@ucd.ie

1. Highlight

Active root exudation of arsenic-phytochelatin complexes in white lupin provides evidence of a new mechanism of arsenic efflux in plants, providing novel pathways for phytoremediation and food safety.

2. Abstract

Arsenic contamination of soils threatens the health of millions globally through accumulation in crops. While plants detoxify arsenic via phytochelatin (PC) complexation and efflux of arsenite from roots, arsenite efflux mechanisms are not fully understood. Here, white lupin (*Lupinus albus*) was grown in semi-hydroponics and exudation of glutathione (GSH) derivatives and PCs in response to arsenic was scrutinised using LC-MS/MS. Inhibiting synthesis of PC precursor GSH with L-buthionine sulfoximine (BSO) or ABC transporters with vanadate drastically reduced (>22%) GSH-derivative and PC_2 exudation, but not PC_3 exudation. This was accompanied by arsenic hypersensitivity in plants treated with BSO and moderate sensitivity with vanadate treatment. Investigating arsenic-phytochelatin (As-PC) complexation revealed two distinct As-PC complexes, As bound to GSH and PC_2 (GS-As-PC_2) and As bound to PC_3 (As-PC_3), in exudates of As-treated lupin. Vanadate inhibited As-PC exudation, while BSO inhibited both the synthesis and exudation of As-PC complexes. These results demonstrate a role of GSH-derivatives and PC exudation in lupin arsenic tolerance and reveal As-PC exudation as a new potential mechanism contributing to active arsenic efflux in plants. Overall, this study uncovers insight into rhizosphere arsenic detoxification with potential to help mitigate pollution and reduce arsenic accumulation in crops.

3. Keywords and abbreviations

Keywords: Lupinus albus; arsenic; arsenic phytochelatin complexes; exclusion; sequestration; phytochelatin; phytoremediation; soil pollution; rhizosphere; root exudates

Abbreviations:

ABC: ATP-binding cassette transporter

AR: arsenate reductase

BSO: L-buthionine sulfoximine

GSH: glutathione

GSSG: glutathione disulfide

HSD: honest significant difference

oxPC: oxidised phytochelatin

PC: phytochelatin

4. Introduction

Arsenic is a major soil contaminant affecting environment and human health. Contamination of soil and groundwater is widespread, with elevated arsenic concentrations resulting from natural weathering and biological activity, as well as anthropogenic activities like mining and agriculture (Patel et al., 2023). With an estimated 2.8 million contaminated sites in Europe and 20 million hectares of farmland affected by heavy metals in China, extensive soil pollution is putting substantial pressure on agricultural soils (FAO & ITPS, 2015). As plants readily take up mobile arsenic from the soil and translocate it to aboveground tissues, dietary intake presents a major exposure route to humans, potentially threatening millions with a range of adverse health effects from arsenic poisoning. In particular, accumulation in major food crops such as rice is an international concern (Zhao et al., 2010a). Therefore, understanding the specific processes governing arsenic bioavailability, uptake, and detoxification in plants is critical for developing mitigation strategies. One crucial plant-soil interaction thought to help plants adapt to and influence arsenic-challenged soil is the release of diverse metabolites from roots (root exudates) which can markedly impact soil chemistry and microbiota to influence contaminant tolerance (Podar & Maathuis, 2022). However, the molecular mechanisms underlying root exudate-mediated arsenic detoxification are not fully elucidated.

In aerobic soils, plants predominantly encounter arsenic in the form of arsenate [As(V)] which enters roots through phosphate transporters (Asher & Reay, 1979; Ullrich-Eberius et al., 1989), while arsenite [As(III)] is most prevalent in anaerobic soils and enters roots through aquaporin channels (Bienert et al., 2008).

Arsenic detoxification in plants involves the reduction of As(V) to As(III) by arsenate reductases such as ACR2 and HAC1, identified in both hyperaccumulating and non-hyperaccumulating plant species (Li et al., 2016). The subsequent tolerance mechanisms have been largely studied in the As hyperaccumulator *Pteris vittata* (Lombi et al., 2002; Ma et al., 2001; Su et al., 2008). In *P. vittata,* the reduced As(III) is rapidly transported to aboveground tissues, where free As(III) is sequestered in vacuoles (Zhao et al., 2009). In contrast, non-hyperaccumulating species preferentially eliminate up to 90 % of internally reduced As(III) back into the external medium, partly through aquaporin channels but also through yet-to-be identified pathways (Zhao et al., 2010b), while the remaining intracellular As(III) is complexed with phytochelatins (Schmöger et al., 2000).

Phytochelatins (PC_n) are oligomers derived from glutathione (GSH) and comprised of (γ-glutamylcysteinyl)$_n$ glycine units, typically with n between 2 and 6. PCs can form stable complexes with arsenic through coordination with cysteine thiol groups, including As-PC_3, As-$(PC_2)_2$ and GS-As-PC_2 (Raab et al., 2004). Other toxic metals like cadmium can also complex with PCs and GSH in a similar manner (Lux et al., 2011). The formation of these complexes play a critical role in metal(loid) detoxification and stabilisation in plants. Liu et al., (2010) found up to 70% of intracellular As(III) bound to PCs in *Arabidopsis thaliana* roots. Mutants deficient in PC synthesis, such as *cad1-3*, exhibit 10- to 20-fold greater sensitivity to arsenate, measured by seedling biomass production, compared to wild-type plants (Ha et al., 1999). Furthermore, inhibition of the PC precursor GSH using L-buthionine sulfoximine (BSO) induces arsenic hypersensitivity across diverse plant species (Meharg & Hartley-Whitaker, 2002).

The ultimate phase of arsenic detoxification in non-hyperaccumulating plants is thought to occur through ATP-dependent vacuolar loading of arsenic-phytochelatin complexes, mediated by ABC

transporters localised to the tonoplast, as evidenced by inhibition of arsenic-phytochelatin vacuolar sequestration with ABC transport inhibitor vanadate (Song et al., 2010). However, recent evidence also points to extracellular roles of PCs in arsenic detoxification. Phytochelatin 2 was found in root exudates of *Lupinus albus*, suggesting arsenic complexation in the rhizosphere or PC complex-mediated efflux of As(III) directly from roots (Frémont et al., 2022). Elucidating the mechanisms and roles of PC exudation is important for harnessing the potential of root exudates to mitigate arsenic environmental and health damage, yet a number of challenging methodological hurdles need to be overcome.

Current methods for capturing root exudates largely utilise hydroponic and aeroponic cultivation systems. While these substrate-free growth methods provide easy access to roots and root exudates, they lack the physical properties of soils that influence root architecture and physiology (Oburger & Jones, 2018). Soil-like substrates such as silica sand may offer advantages, providing mechanical support and resistance to root growth that feedback to modulate root morphology and exudate composition, while still maintaining inert properties to limit interference from soil organic particles (Sasse et al., 2020). Beyond experimental limitations, chemical characterisation of root exudates also faces several hurdles, particularly due to the intricate chemical interactions occurring between arsenic and root exudates, which may produce transient compounds critical for arsenic detoxification (Bluemlein et al., 2009). Analytical approaches like LC-MS/MS have enabled detection of previously unknown metal-organic complexes involved in metal detoxification in the rhizosphere, such as zinc-nicotianamine (Tsednee et al., 2014). Interestingly, similar mechanisms of extracellular metal detoxification have been identified in microbes, which involve the intracellular production and efflux of the arsenic complex 1-arseno-3-phosphoglycerate, providing a novel As detoxification pathway (Chen et al., 2016). Therefore, coupling physiologically relevant growth systems with selective, high-resolution analytical techniques may shed light on specialised plant exudation mechanisms for arsenic detoxification and tolerance.

This research exploits targeted metabolite assessment to elucidate arsenic-responsive phytochelatin synthesis, exudation and arsenic-phytochelatin complexation in lupin. Chemical inhibition of glutathione synthesis with BSO and ABC transporter-mediated exudation with vanadate are then used to elucidate complex exudation mechanisms and how they influence arsenic fate in the rhizosphere.

5. Materials and methods

5.1 Plant growth and experimental design

Seeds of white lupin (*Lupinus albus* L. cv. AMIGA) were surface sterilised by sequential immersion in 70% ethanol, 1% sodium hypochlorite, and sterile Milli-Q water. Sterilised seeds were germinated on moist filter paper for 3 days, after which seedlings were transferred to growth pouches (7.6 x 15.2 cm) containing 700 ml sterile silica sand, for a total of 30 plants divided into 5 blocks (Fig. 1A). Plants were supplied twice weekly with 65 ml Hoagland nutrient solution (pH 6.0) containing the following concentrations: 600 µM KNO_3, 400 µM $Ca(NO_3)_2{\cdot}4H_2O$, 200 µM $NH_4H_2PO_4$, 100 µM $MgSO_4{\cdot}7H_2O$, 5 µM KCl, 2,5 µM H_3BO_3, 0,2 µM $MnSO_4{\cdot}H_2O$, 0,2 µM $ZnSO_4{\cdot}7H_2O$, 0,05 µM $CuSO_4{\cdot}5H_2O$, 0,05 µM H_2MoO_4, 4,5 µM Fe·Na·EDTA. Growth chamber conditions were 18 h photoperiod under LED lighting (150 µmol m^{-2} s^{-1}) at 25°C. At day 23 after planting, plants were either kept as untreated controls or subjected to BSO or vanadate inhibitor treatments (n=10 each) prepared in Hoagland solution: 0.5 mM L-buthionine sulfoximine (BSO) (>99% Thermo Fisher Scientific, Cat# AC235520010), a GSH synthesis inhibitor (Liu et al., 2010), and 1 mM vanadate (Sodium Orthovanadate, >99% Thermo Fisher Scientific, Cat#

AC205330500) an ABC-type transporter inhibitor (Song, Mendoza-Cózatl, et al., 2014). At day 26 after planting, plants were subjected to a second inhibitor treatment and further divided into + or – arsenate groups with the addition of 13 µM arsenate ($Na_2HAsO_4 \cdot 7H_2O$, Sodium hydrogen arsenate heptahydrate, >98%, Thermo Fisher Scientific, Cat# AAA1827536), resulting in six treatments (n=5 each): control, arsenate, BSO, arsenate + BSO, vanadate, and arsenate + vanadate (Fig. 1A). Unplanted controls were also included for each treatment (n=5 each). Stomatal conductance was measured at day 27 and day 28 (24h and 48 h after As addition, respectively) on the abaxial surface of the youngest fully expanded leaf (Vezza et al., 2018) using a porometer (LI-600, LI-COR Biosciences). At harvest, 28 days after planting, shoot and root morphology, biomass, and root exudates were assessed.

5.2 Root exudate collection and root metabolite extraction

Root exudates were collected following the procedure of Frémont et al. (2022). Briefly, nylon mesh growth pouches were opened and loose sand was gently removed, leaving intact root systems with attached rhizosheaths. Root systems were then immersed in 40 mL Milli-Q water for 10 seconds with gentle circular agitation to collect exudates (Fig. 1B). Although some cellular injury may occur during sampling, this collection method was extensively validated to preclude artifact from damage, as previously demonstrated (Frémont et al., 2022). For unplanted controls, 20 g of sand from each unplanted pot was extracted under identical conditions to mirror the quantity of sand obtained from rhizosheaths. Solutions were lyophilised and stored at -70°C. All lyophilised extracts were resuspended in 800 µL Milli-Q water and 0.1% formic acid, filtered through 0.2 µm centrifuge filters (InnoSep Spin, Canadian Life Sciences) at 10,000 x g for 30 seconds, transferred to HPLC vials and kept at 4°C before LC-MS/MS analysis within 24 h.

After rhizosphere extraction, whole root systems went through 5 additional wash cycles in Milli-Q water with strong vortexing at maximum speed to recover root samples devoid of rhizosphere residues for endosphere metabolite extraction. Root samples were dried of residual water using absorbing paper, immediately frozen in liquid nitrogen, lyophilised, and kept at -70°C. Root samples were ground using a mortar and pestle and 50 mg of dried material was extracted in 1 mL Milli-Q water + 0.1% formic acid for 15 minutes with ultrasonication at 4°C. Endosphere extracts were then centrifuged at 4°C at 20,000 x g for 2 minutes, the supernatant transferred to 0.2 µm centrifuge filters, centrifuged at 10,000 x g for 30 seconds, transferred to HPLC vials and kept at 4°C before LC-MS/MS analysis within 24 h.

5.3 Liquid chromatography-tandem mass spectrometry (LC-MS/MS) analysis

Targeted metabolite profiling was performed using an Agilent 1,260 Infinity HPLC system coupled to an Agilent 6530 Q-TOF mass spectrometer with Jet Stream ionisation source. Chromatographic separation utilised a Zorbax Eclipse Plus C18 column (4.6 x 100 mm, 3.5 µm) at 30°C with a 0.4 mL/min flow rate. The 80 min gradient consisted of solvent A (5% methanol, 0.1% formic acid in water) and solvent B (methanol, 0.1% formic acid), starting at 100% A for 20 min, increasing linearly to 100% B over 50 min, then holding at 100% B for 10 min. Biological samples (n=30), unplanted controls (n=15), and Milli-Q water blanks (n=5) were analysed in ESI+ mode. MS^2 fragmentation used a precursor ion inclusion list at 20 and 35 eV collision energy (Table S1) and was performed on 3 samples per treatment (n= 18). Source parameters included 300°C gas temperature, 5 L/min drying gas, 45 psig nebulizer pressure, 250°C sheath gas temperature, and 11 L/min sheath gas flow.

LC-MS raw data were processed in MZmine 3.4.14 (Schmid et al., 2023). Background noise was filtered at intensity thresholds of 800 for MS^1 and 10 for MS^2. Chromatograms were constructed within 10 ppm mass accuracy and minimum peak intensity of 800. Extracted ion chromatograms were deconvoluted using MZmine's minimum search algorithm. Isotope peaks were grouped within 10 ppm mass tolerance and 0.1 min retention time tolerance. Features were aligned across samples within 15 ppm mass tolerance (75% weighting) and 0.2 min retention time tolerance (25% weighting). Features containing MS^2 spectra were retained. Gaps in the feature matrix were filled within 0.8 min retention time and 5 ppm mass tolerances. MS^2 spectra were matched to precursor ions within 0.02 m/z and 0.2 min retention time windows. MS^2 spectra acquired at 20 and 35 V collision energies were merged into consensus spectra after summing their intensities.

5.4 Targeted metabolite annotation

Targeted features were annotated as glutathione (GSH), glutathione disulfide (GSSG), phytochelatins (PCs) and their arsenic (As) complexes based on matching retention times and MS^2 spectra (cosine > 0.8) to those of authentic standards analysed under identical LC-MS/MS conditions (Fig. 1B). The analytical work conducted here also does not discount compound transformation during sampling, such as the potential oxidation of GSH into GSSG, which could be collectively considered here as changes in total glutathione (but does not alter any conclusion presented). Standards were prepared from commercially obtained phytochelatin 2 (PC_2) and phytochelatin 3 (PC_3) (Anaspec, Fremont, CA, USA), GSH (Alfa Aesar Co., Inc., Ward Hill, MA, USA) and GSSG (ACROS Organics, Geel, Belgium). Oxidised PCs were generated via spontaneous oxidation during sample preparation. As-PC complexes were synthesised following Schmied-Tobies et al. (2014) by incubating PC_2, PC_3 and GSH standards (100 µM) with arsenite at various thiol (SH):As molar ratios (3:1, 1:3, 1:6) in 0.1% formic acid. To synthesise As-GS_3 complex, GSH alone was incubated with As (III) at a 1:6 SH:As molar ratio. See Supporting Information Table S1 for the full list of ions produced from As-PC *in vitro* complexation and their corresponding chemical formulas.

5.5 Statistical analysis

One-way analysis of variance (ANOVA) followed by Tukey's honest significant difference (HSD) *post hoc* test was used to determine treatment effects when data met assumptions of normality and homogeneity of variance. For non-normal or heteroscedastic data, the non-parametric Kruskal-Wallis test followed by Dunn's *post hoc* test was used for multiple comparisons. P values were adjusted for false discovery rate control using the Benjamini-Hochberg method (Benjamini & Hochberg, 1995). Pairwise comparisons were performed using T-tests when data met assumptions of normality and homogeneity of variance and Mann-Whitney U tests for non-normal or heteroscedastic data. All analyses were conducted in R v.4.3.1 (R Core Team, 2020).

6. Results

6.1 Physiological response

Lupin plants (*Lupinus albus*) were left either as untreated controls, or subjected to treatments with arsenic (As), L-buthionine sulfoximine (BSO), As + BSO, vanadate, or As + vanadate. Stomatal conductance (g_s) was measured 27 and 28 days after planting (24 and 48 hours after As addition, respectively). On day 27, neither As nor inhibitor treatments significantly affected g_s, except for a significant decrease from 0.25 ± 0.043 to 0.04 ± 0.01 mol m^{-2} s^{-1} with As + BSO compared to As alone

(P<0.05, ANOVA, Tukey's HSD; Fig. 2B). By day 28, no significant effects on g_s were observed for As, BSO or vanadate alone. However, As + BSO significantly reduced g_s to undetectable levels compared to 0.12 ± 0.026 mol m^{-2} s^{-1} in controls and 0.18 ± 0.036 mol m^{-2} s^{-1} in As-treated plants, and wilting was observed, while As + vanadate significantly decreased g_s to 0.03 ± 0.01 mol m^{-2} s^{-1} compared to As alone, without any observable morphological effects (Fig. 2A, B). At harvest on day 28, only As + BSO reduced shoot fresh biomass compared to controls, from 3,596 ± 305 mg FW in controls to 2,501 ± 98 mg FW in As + BSO (P<0.05, ANOVA, Tukey's HSD).

6.2 Targeted analysis of glutathione and phytochelatin exudates

To evaluate the metabolic response of lupin to arsenic, root tissue (endosphere) extracts and rhizosphere exudates from arsenic-treated plants were analysed using LC-MS/MS and compared to authentic standards. Six major glutathione-derived compounds and phytochelatins (PCs) were measured: glutathione (GSH), glutathione disulfide (GSSG), phytochelatin 2 (PC_2), oxidised phytochelatin 2 ($oxPC_2$), phytochelatin 3 (PC_3) and two isomers of oxidised phytochelatin 3 ($oxPC_3$, iso-$oxPC_3$). The endosphere contained GSH, GSSG, both reduced and oxidised forms of PC_2, but only $oxPC_3$ (Fig. 3A). Exudates contained GSH, GSSG, $oxPC_2$ and $oxPC_3$. $OxPC_2$ was most prominent in both the endosphere and rhizosphere of arsenic-treated plants.

In comparing endosphere of control and arsenic-treated plants, GSH levels were not significantly different, while GSSG was depleted in As-treated roots (Fig. 3B). PC_2 was detected in As-treated plants but not in controls, while PC_3 was not detected. $OxPC_2$ and $oxPC_3$ were enriched in As-treated roots compared to controls, with iso-$oxPC_3$ not detected in controls (Fig. 3B). In exudates, GSH did not significantly vary between controls and As-treated plants, while GSSG was significantly depleted (Fig. 3C). Exuded $oxPC_2$ and $oxPC_3$ were enriched in As-treated plants compared to controls, with $oxPC_2$ the most enriched compound, and iso-$oxPC_3$ absent in untreated controls (Fig. 3C).

6.3 Inhibition of arsenic response

In the endosphere, co-treatment with As + BSO did not significantly alter levels of GSH, GSSG, PC_2 and $oxPC_2$ compared to As alone (Fig. 3B). However, $oxPC_3$ and iso-$oxPC_3$ were significantly depleted with As + BSO co-treatment compared to As alone. Compared to controls, GSH, PC_2, $oxPC_2$, $oxPC_3$ and iso-$oxPC_3$ were significantly enriched in As + BSO co-treatment, while GSSG did not significantly vary. Co-treatment with As + vanadate resulted no significant change in levels of GSH, PC_2, $oxPC_2$, $oxPC_3$ and iso-$oxPC_3$ compared to As alone but induced a significant enrichment of GSSG. Compared to control, As + vanadate significantly increased GSH, $oxPC_2$, $oxPC_3$ and iso-$oxPC_3$ but did not significantly affect levels of GSSG or PC_2.

In exudates, co-treatment with As + BSO significantly reduced As response of the thiol-containing compounds, with GSH, GSSG and $oxPC_3$ being depleted compared to both control and As treatment, while $oxPC_2$ and iso-$oxPC_3$ returned to control levels (Fig. 3C). Co-treatment with As + vanadate did not significantly alter GSH, GSSG, $oxPC_3$ and iso-$oxPC_3$ levels compared to As-treatment, but did significantly deplete levels of $oxPC_2$. Compared to controls, As + vanadate co-treatment resulted in similar levels of GSH and a significantly depleted level of GSSG, as well as significantly increased levels of $oxPC_2$, $oxPC_3$ and iso-$oxPC_3$ (Fig. 3C).

6.4 Targeted analysis of arsenic-phytochelatin complexes in exudates

To evaluate the potential for detecting arsenic-phytochelatin (As-PC) complexes in the endosphere and root exudates, an *in vitro* experiment was conducted in which arsenite As(III) was incubated in 0.1 M formic acid with standards of GSH, PC_2, and PC_3, either individually or in combinations at varying thiol:arsenic molar ratios. LC-MS/MS revealed six chromatographic peaks present only with As addition, corresponding to five distinct As-PC complexes and their isomers (Fig. 4A, Table S1).

By re-analysing endosphere and exudate samples with these *in vitro*-derived spectra (Fig. 4a), two As-PC complexes were identified in both endosphere and exudates: GS-As-PC_2, which comprised one molecule of GSH and one molecule of PC_2 coordinated to As(III) through their three thiol groups, and As-PC_3, in which As(III) is coordinated to the three thiol groups of one PC_3 molecule (Fig. 4B). GS-As-PC_2 and As-PC_3 were absent from control endosphere and exudate samples and As-PC_3 was the most prevalent As complex in As-treated endosphere and exudates (Fig. 4C, D).

In the endosphere, addition of BSO significantly reduced levels of both GS-As-PC_2 and As-PC_3 compared to As treatment alone, while vanadate had no significant effect on endosphere GS-As-PC_2 and As-PC_3 levels compared to As treatment alone (Fig. 4C). However, both the application of BSO and the application of vanadate eliminated all GS-As-PC_2 from exudates, while As-PC_3 exudation was only partially reduced with BSO, and almost eliminated with vanadate, with only one outlier with detectable As-PC_3 (Fig. 4C, D).

7. Discussion

7.1 Combination of metabolic inhibitors and arsenic disrupts lupin arsenic tolerance

Arsenic (As) alone had no significant effect on stomatal conductance or biomass in lupin, which confirms tolerance to short-term exposure to 13 µM As(V) as previously observed (Frémont et al., 2022; Vázquez et al., 2005). Similarly, the application of inhibitors without arsenic treatment did not affect physiological parameters compared to control, except for a small non-significant increase in stomatal conductance 24 h after L-buthionine sulfoximine (BSO) treatment, indicating physiological functions were largely maintained during inhibitor treatment. However, co-treatment with As and BSO, which inhibits glutathione (GSH) synthesis (Liu et al., 2010), substantially reduced both stomatal conductance and biomass, particularly after 48 h, with complete loss of stomatal conductance and wilting (Fig. 2). This acute sensitivity to As + BSO co-treatment resembles the response previously reported with much higher (5×) As concentrations (Frémont et al., 2022), underscoring the protective role of GSH and derivatives in mitigating arsenic toxicity in lupin. Additionally, co-treatment with As and vanadate, an ATP-dependent membrane transport inhibitor (Song, et al., 2014), decreased stomatal conductance at 48 h, highlighting vanadate-induced As sensitivity and suggesting the involvement of active transmembrane transport in lupin As detoxification.

7.2 Targeted exudates assessment reveals critical roles of glutathione-derived metabolites and phytochelatin synthesis and exudation in lupin arsenic tolerance

In a previous study, Frémont et al., (2022) reported the presence of PCs in exudates of arsenic-treated lupin plants. Since PCs are major arsenic detoxification metabolites in plants (Cobbett & Goldsbrough, 2002), the exudation of PCs and their GSH precursor were examined here to gain insight into their

mechanisms of exudation, interactions with arsenic and roles in As detoxification. With the exception of GSH, which was unchanged, all measured GSH-derivatives and PCs in endosphere and exudates exhibited significant and substantial responses to As addition compared to controls (Fig. 3). Oxidised glutathione (GSSG) decreased by 8% in the endosphere and 17% in arsenic-treated exudates. Since GSH is challenging to capture in exudates owing to its high reactivity (Giustarini et al., 2016), the significant GSSG depletion is an important clue indicating a general shift of the glutathione pathway towards increased PC synthesis in response to arsenic (Frémont et al., 2022; Vázquez et al., 2005). Oxidised PCs ($oxPC_2$ and $oxPC_3$) increased in abundance by >30% in the endosphere and >60% in exudates, confirming the enriched synthesis and exudation of $oxPC_2$ in response to As reported by Frémont et al., (2022) and the novel detection of $oxPC_3$ in lupin exudates.

Surprisingly, while As + BSO co-treatment significantly decreased GSH exudation, it did not decrease GSH levels in the endosphere (Fig. 3B), contradictory with the target role of BSO as endogenous GSH synthesis inhibitor (Liu et al., 2010). An explanation for this could be that absolute production levels of GSH were reduced but concentrations were inflated against the resulting reduced growth. Another possible explanation could be the reduction of GSH exudation, compensating for the BSO-mediated reduction in endogenous GSH synthesis in order to maintain GSH levels within roots. Different responses between endosphere and exudates were also observed for GSSG and $oxPC_2$, which remained unchanged in the endosphere but were drastically reduced in exudates upon addition of As + BSO co-treatment (Fig. 3C), suggesting a reduced GSH availability affecting exudation of metabolites downstream from GSH, such as GSSG, and PCs. On the other hand, the significant depletion of $oxPC_3$ in the endosphere and in exudates with As + BSO co-treatment indicates decreased PC_3 synthesis and exudation. As PC_3 is a product of the stepwise condensation of γ-Glu-Cys moieties to PC_2 itself and of the growing phytochelatin chain, its synthesis is dependent on the availability of both PC_2 and GSH (Grill et al., 1989), which is likely strongly compromised with the addition of As + BSO. The severe disruption of lupin As tolerance with As + BSO observed here (Fig. 2) suggests inhibiting GSH synthesis likely disrupted PC production and exudation, which compromised essential As detoxification mechanisms such as the chelation of As(III) into non-toxic As-PCs complexes.

Inhibition of ATP-dependant membrane transport with vanadate effectively reduced exudate levels of $oxPC_2$ by more than 22% but did not influence endogenous synthesis (Fig. 3). This indicates active transport and exudation of $oxPC_2$ across membranes likely involves (ATP-dependant) ABC transporters, analogous to those involved in As-PC complex loading into vacuoles in *Arabidopsis thaliana* (Song et al., 2010). However, unaltered levels of $oxPC_3$ in endosphere and exudates after As + vanadate treatment suggests a different exudation route may exist for these compounds. Collectively, although plasma membrane ABC transport appears important to facilitate $oxPC_2$ exudation, this alone may not fully explain the observed As-sensitivity with As-vanadate co-treatment (Fig. 2) but likely represents one of multiple arsenic detoxification mechanisms conferring lupin As-tolerance, which potentially include As-PC complex exudation.

7.3 Phytochelatin-arsenic complexes exudation provides a new route for arsenic efflux and detoxification in lupin

Characterising arsenic-phytochelatin (As-PC) complexes in plant matrices presents several analytical challenges (Bluemlein et al., 2008, 2009) and is even more difficult in complex extracellular environments like the rhizosphere. To target specific As-PCs in the endosphere and the rhizosphere, As-PC complexes were first synthesised in vitro from GSH, PC_2, and PC_3 and analysed using LC-MS/MS (Fig. 4A). Five distinct As-PC species were detected, representing all known As-PC coordination schemes from these three compounds (Bluemlein et al., 2009; Schmied-Tobies et al., 2014). A targeted search for these complexes in endosphere and exudates of As treated plants revealed the presence of two As-PC complexes (Fig. 4A, B), indicating rhizosphere As complexation, or As-complex exudation from roots, may act as a yet unknown As-detoxification mechanism in lupin.

Using this As-PC complex fingerprint, complexation in the rhizosphere was also explored after the use of detoxification inhibitors. By disrupting GSH synthesis, BSO also interrupted or drastically reduced As-PC in the endosphere and in exudates (Fig. 4C, D), indicating that arsenic detoxification through As-PC complex formation relies on the availability of GSH for PC synthesis and As binding (Grill et al., 1989). Conversely, vanadate treatment had no effect on endosphere As-PC levels but abolished As-PC complexes in exudates (Fig 4C, D), likely due to inactivation of target membrane ABC-type transporters. This provides evidence of As-PC exudation as an active process, potentially occurring via ATP-dependant ABC transporters, similar to those plants use for As-PC vacuolar loading and sequestration (Song et al., 2010) (Fig. 5). In *Arabidopsis thaliana* and *Oryza sativa*, As-PC transport from the cytosol to the vacuole is mediated by an ABCC type transporter system (Song et al., 2010; 2014). These transporters may also mediate As-PC exudation to the rhizosphere, as suggested by the immunofluorescence localisation of ABCC transporters to outer root cell layers in Song et al. (2014). This new route for As detoxification in lupin may provide an additional mechanism beyond the current understanding of As(III) efflux from roots, of which approximately 20% is explained by NIP transporter-mediated efflux of free As(III), while the remaining 80% is still unaccounted for (Zhao et al., 2010b). While there is some evidence of increased unbound As(III) efflux when PC production is compromised (Liu et al., 2010), to our knowledge, this is the first investigation and report of As-phytochelatin complexes in exudates and characterisation of the exudation mechanisms involved.

7.4 Limitations and future work

Accurate sampling and assessment of root exudate compounds can be challenging due to the complexity of rhizosphere environments, the wide diversity and low concentrations of metabolites, and technical limitations in detection and quantification methods (Escolà Casas & Matamoros, 2021; Salem et al., 2022), particularly for potentially transient exuded As-PC complexes. Contemporary metabolite assessment approaches rely on direct comparison of spectra for accurate detection of metabolite changes between treatments in complex sample matrices, but provide limited insight into the relative contribution of a metabolite to a specific putative functional pathway. Estimated absolute concentrations of PCs and As-PC (Table S2) provide some further insight into the potential As detoxification contribution. Determining the proportional contribution of an As-PC exudation pathway to arsenic detoxification and arsenic speciation dynamics in the rhizosphere is an exciting research priority raised by these findings, in order to reveal the potential to influence metal tolerance. Similarly,

future studies should explore if this pathway is conserved in other crops, model organisms, and with other metals.

These findings indicate As-PC complexes may contribute to As(III) efflux from roots, providing a new As detoxification and tolerance mechanism in plants. In addition to potentially contributing to the 80% of previously unexplained As(III) exudation from roots (Zhao et al., 2010b), this pathway may have different specificity for arsenic (and other toxic metals like cadmium) compared to aquaporin channels. Ultimately, a better understanding of this new pathway and its contribution to overall arsenic detoxification could help optimisation of phytoremediation applications and inform strategies aimed at reducing arsenic accumulation in food crops.

8. Acknowledgements

We would like to thank Dr. Benjamin Péret for graciously providing white lupin seeds. A special thank you is extended to Ariane Lafrenière for her kind support during harvest.

9. Author contributions

AF, NB, ES, FP, and JB conceived the study. MS performed the LC-MS/MS analysis. AF performed the data analysis and drafted the manuscript. ES, NB, FP, MS, and JB participated in data analysis and discussion. All authors contributed to writing and editing the final manuscript.

10. Conflict of interest

No conflict of interest declared.

11. Funding

This work was supported by NSERC Discovery Grant (FEP RGPIN-2017-05452), MITACS (IT23193), NSERC/Hydro-Québec Industrial Research Chair in Phytotechnology, and the UCD Ad Astra Fellowship Programme.

12. Data availability

All primary data to support the findings of this study were deposited to MassIVE and are openly available at [http://massive.ucsd.edu; MSV000093078]. Spectra from As-PC in vitro complexation were added as new library entries on the Global Natural Products Social Molecular Networking (GNPS) platform (https://gnps.ucsd.edu), and spectra IDs are listed in Supplementary Information Table S1.

References

Asher, C. J., & Reay, P. F. (1979). Arsenic Uptake by Barley Seedlings. *Functional Plant Biology*, *6*(4), 459–466. https://doi.org/10.1071/pp9790459

Benjamini, Y., & Hochberg, Y. (1995). Controlling the False Discovery Rate: A Practical and Powerful Approach to Multiple Testing. *Journal of the Royal Statistical Society: Series B (Methodological)*, *57*(1), 289–300. https://doi.org/10.1111/j.2517-6161.1995.tb02031.x

Bienert, G. P., Thorsen, M., Schüssler, M. D., Nilsson, H. R., Wagner, A., Tamás, M. J., & Jahn, T. P. (2008). A subgroup of plant aquaporins facilitate the bi-directional diffusion of As(OH)3 and Sb(OH)3across membranes. *BMC Biology*, *6*(1), 26. https://doi.org/10.1186/1741-7007-6-26

Bluemlein, K., Raab, A., & Feldmann, J. (2009). Stability of arsenic peptides in plant extracts: Off-line versus on-line parallel elemental and molecular mass spectrometric detection for liquid chromatographic separation. *Analytical and Bioanalytical Chemistry*, *393*(1), 357–366. https://doi.org/10.1007/s00216-008-2395-z

Bluemlein, K., Raab, A., Meharg, A. A., Charnock, J. M., & Feldmann, J. (2008). Can we trust mass spectrometry for determination of arsenic peptides in plants: Comparison of LC–ICP–MS and LC–ES-MS/ICP–MS with XANES/EXAFS in analysis of Thunbergia alata. *Analytical and Bioanalytical Chemistry*, *390*(7), 1739–1751. https://doi.org/10.1007/s00216-007-1724-y

Chen, J., Yoshinaga, M., Garbinski, L. D., & Rosen, B. P. (2016). Synergistic interaction of glyceraldehydes-3-phosphate dehydrogenase and ArsJ, a novel organoarsenical efflux permease, confers arsenate resistance. *Molecular Microbiology*, *100*(6), 945–953. https://doi.org/10.1111/mmi.13371

Cobbett, C., & Goldsbrough, P. (2002). Phytochelatins and Metallothioneins: Roles in Heavy Metal Detoxification and Homeostasis. *Annual Review of Plant Biology*, *53*(1), 159–182. https://doi.org/10.1146/annurev.arplant.53.100301.135154

Escolà Casas, M., & Matamoros, V. (2021). Analytical challenges and solutions for performing metabolomic analysis of root exudates. *Trends in Environmental Analytical Chemistry*, *31*, e00130. https://doi.org/10.1016/j.teac.2021.e00130

FAO, & ITPS. (2015). Status of the world's soil resources: Main Report. *FAO & ITPS*. http://www.fao.org/3/ a-i5199e.pdf

Frémont, A., Sas, E., Sarrazin, M., Gonzalez, E., Brisson, J., Pitre, F. E., & Brereton, N. J. B. (2022). Phytochelatin and coumarin enrichment in root exudates of arsenic-treated white lupin. *Plant, Cell & Environment*, *45*(3), 936–954. https://doi.org/10.1111/pce.14163

Giustarini, D., Tsikas, D., Colombo, G., Milzani, A., Dalle-Donne, I., Fanti, P., & Rossi, R. (2016). Pitfalls in the analysis of the physiological antioxidant glutathione (GSH) and its disulfide (GSSG) in biological samples: An elephant in the room. *Journal of Chromatography B*, *1019*, 21–28. https://doi.org/10.1016/j.jchromb.2016.02.015

Grill, E., Löffler, S., Winnacker, E.-L., & Zenk, M. H. (1989). Phytochelatins, the heavy-metal-binding peptides of plants, are synthesized from glutathione by a specific γ-

glutamylcysteine dipeptidyl transpeptidase (phytochelatin synthase). *Proceedings of the National Academy of Sciences*, *86*(18), 6838–6842. https://doi.org/10.1073/pnas.86.18.6838

Ha, S.-B., Smith, A. P., Howden, R., Dietrich, W. M., Bugg, S., O'Connell, M. J., Goldsbrough, P. B., & Cobbett, C. S. (1999). Phytochelatin Synthase Genes from Arabidopsis and the Yeast Schizosaccharomyces pombe. *The Plant Cell*, *11*(6), 1153–1163. https://doi.org/10.1105/tpc.11.6.1153

Li, N., Wang, J., & Song, W.-Y. (2016). Arsenic Uptake and Translocation in Plants. *Plant and Cell Physiology*, *57*(1), 4–13. https://doi.org/10.1093/pcp/pcv143

Liu, W.-J., Wood, B. A., Raab, A., McGrath, S. P., Zhao, F.-J., & Feldmann, J. (2010). Complexation of Arsenite with Phytochelatins Reduces Arsenite Efflux and Translocation from Roots to Shoots in Arabidopsis. *Plant Physiology*, *152*(4), 2211–2221. https://doi.org/10.1104/pp.109.150862

Lombi, E., Zhao, F.-J., Fuhrmann, M., Ma, L. Q., & McGrath, S. P. (2002). Arsenic distribution and speciation in the fronds of the hyperaccumulator Pteris vittata. *New Phytologist*, *156*(2), 195–203. https://doi.org/10.1046/j.1469-8137.2002.00512.x

Lux, A., Martinka, M., Vaculík, M., & White, P. J. (2011). Root responses to cadmium in the rhizosphere: A review. *Journal of Experimental Botany*, *62*(1), 21–37. https://doi.org/10.1093/jxb/erq281

Ma, L. Q., Komar, K. M., Tu, C., Zhang, W., Cai, Y., & Kennelley, E. D. (2001). A fern that hyperaccumulates arsenic. *Nature*, *409*(6820), 579–579. https://doi.org/10.1038/35054664

Meharg, A. A., & Hartley-Whitaker, J. (2002). Arsenic uptake and metabolism in arsenic resistant and nonresistant plant species: Tansley review no. 133. *New Phytologist*, *154*(1), 29–43. https://doi.org/10.1046/j.1469-8137.2002.00363.x

Oburger, E., & Jones, D. L. (2018). Sampling root exudates – Mission impossible? *Rhizosphere*, *6*, 116–133. https://doi.org/10.1016/j.rhisph.2018.06.004

Patel, K. S., Pandey, P. K., Martín-Ramos, P., Corns, W. T., Varol, S., Bhattacharya, P., & Zhu, Y. (2023). A review on arsenic in the environment: Contamination, mobility, sources, and exposure. *RSC Advances*, *13*(13), 8803–8821. https://doi.org/10.1039/D3RA00789H

Podar, D., & Maathuis, F. J. M. (2022). The role of roots and rhizosphere in providing tolerance to toxic metals and metalloids. *Plant, Cell & Environment*, *45*(3), 719–736. https://doi.org/10.1111/pce.14188

R Core Team. (2020). *R: A Language and Environment for Statistical Computing* [Computer software]. https://www.R-project.org/

Raab, A., Feldmann, J., & Meharg, A. A. (2004). The Nature of Arsenic-Phytochelatin Complexes in Holcus lanatus and Pteris cretica. *Plant Physiology*, *134*(3), 1113–1122. https://doi.org/10.1104/pp.103.033506

Salem, M. A., Wang, J. Y., & Al-Babili, S. (2022). Metabolomics of plant root exudates: From sample preparation to data analysis. *Frontiers in Plant Science*, *13*. https://doi.org/10.3389/fpls.2022.1062982

Sasse, J., Kosina, S. M., Raad, M. de, Jordan, J. S., Whiting, K., Zhalnina, K., & Northen, T. R. (2020). Root morphology and exudate availability are shaped by particle size and chemistry in Brachypodium distachyon. *Plant Direct*, *4*(7), e00207. https://doi.org/10.1002/pld3.207

Schmid, R., Heuckeroth, S., Korf, A., Smirnov, A., Myers, O., Dyrlund, T. S., Bushuiev, R., Murray, K. J., Hoffmann, N., Lu, M., Sarvepalli, A., Zhang, Z., Fleischauer, M., Dührkop, K., Wesner, M., Hoogstra, S. J., Rudt, E., Mokshyna, O., Brungs, C., … Pluskal, T. (2023). Integrative analysis of multimodal mass spectrometry data in MZmine 3. *Nature Biotechnology*, 1–3. https://doi.org/c

Schmied- Tobies, M. I. H., Arroyo- Abad, U., Mattusch, J., & Reemtsma, T. (2014). Mass spectrometric detection, identification, and fragmentation of arseno-phytochelatins. *Journal of Mass Spectrometry*, *49*(11), 1148–1155. https://doi.org/10.1002/jms.3435

Schmöger, M. E. V., Oven, M., & Grill, E. (2000). Detoxification of Arsenic by Phytochelatins in Plants. *Plant Physiology*, *122*(3), 793–802.

Song, W.-Y., Mendoza-Cózatl, D. G., Lee, Y., Schroeder, J. I., Ahn, S.-N., Lee, H.-S., Wicker, T., & Martinoia, E. (2014). Phytochelatin–metal(loid) transport into vacuoles shows different substrate preferences in barley and Arabidopsis. *Plant, Cell & Environment*, *37*(5), 1192–1201. https://doi.org/10.1111/pce.12227

Song, W.-Y., Park, J., Mendoza-Cózatl, D. G., Suter-Grotemeyer, M., Shim, D., Hörtensteiner, S., Geisler, M., Weder, B., Rea, P. A., Rentsch, D., Schroeder, J. I., Lee, Y., & Martinoia, E. (2010). Arsenic tolerance in Arabidopsis is mediated by two ABCC-type phytochelatin transporters. *Proceedings of the National Academy of Sciences*, *107*(49), 21187–21192. https://doi.org/10.1073/pnas.1013964107

Song, W.-Y., Yamaki, T., Yamaji, N., Ko, D., Jung, K.-H., Fujii-Kashino, M., An, G., Martinoia, E., Lee, Y., & Ma, J. F. (2014). A rice ABC transporter, OsABCC1, reduces arsenic accumulation in the grain. *Proceedings of the National Academy of Sciences*, *111*(44), 15699–15704. https://doi.org/10.1073/pnas.1414968111

Su, Y. H., McGrath, S. P., Zhu, Y. G., & Zhao, F. J. (2008). Highly efficient xylem transport of arsenite in the arsenic hyperaccumulator Pteris vittata. *New Phytologist*, *180*(2), 434–441. https://doi.org/10.1111/j.1469-8137.2008.02584.x

Tsednee, M., Yang, S.-C., Lee, D.-C., & Yeh, K.-C. (2014). Root-Secreted Nicotianamine from Arabidopsis halleri Facilitates Zinc Hypertolerance by Regulating Zinc Bioavailability. *Plant Physiology*, *166*(2), 839–852. https://doi.org/10.1104/pp.114.241224

Ullrich-Eberius, C. I., Sanz, A., & Novacky, A. J. (1989). Evaluation of Arsenate- and Vanadate-Associated Changes of Electrical Membrane Potential and Phosphate Transport in Lemna gibba G1. *Journal of Experimental Botany*, *40*(1), 119–128. https://doi.org/10.1093/jxb/40.1.119

Vázquez, S., Esteban, E., & Goldsbrough, P. (2005). Arsenate-induced phytochelatins in white lupin: Influence of phosphate status. *Physiologia Plantarum*, *124*(1), 41–49. https://doi.org/10.1111/j.1399-3054.2005.00484.x

Vezza, M. E., Llanes, A., Travaglia, C., Agostini, E., & Talano, M. A. (2018). Arsenic stress effects on root water absorption in soybean plants: Physiological and morphological aspects. *Plant Physiology and Biochemistry*, *123*, 8–17. https://doi.org/10.1016/j.plaphy.2017.11.020

Zhao, F.-J., Ago, Y., Mitani, N., Li, R.-Y., Su, Y.-H., Yamaji, N., McGrath, S. P., & Ma, J. F. (2010). The role of the rice aquaporin Lsi1 in arsenite efflux from roots. *New Phytologist*, *186*(2), 392–399. https://doi.org/10.1111/j.1469-8137.2010.03192.x

Zhao, F.-J., McGrath, S. P., & Meharg, A. A. (2010). Arsenic as a Food Chain Contaminant: Mechanisms of Plant Uptake and Metabolism and Mitigation Strategies. *Annual Review of Plant Biology*, *61*(1), 535–559. https://doi.org/10.1146/annurev-arplant-042809-112152

Zhao, Ma, J. F., Meharg, A. A., & McGrath, S. P. (2009). Arsenic uptake and metabolism in plants. *New Phytologist*, *181*(4), 777–794. https://doi.org/10.1111/j.1469-8137.2008.02716.x

13. Tables

Empty

14. Figure legends

Fig. 1 Experimental design and workflow for collecting and analysing root exudates. **(A)** Experimental design (n = 5, illustrated; total plants = 30), with each plant grown for 22 days before inhibitors, arsenic, and co-treatments. **(B)** Exudate capture workflow, adapted from Frémont et al. (2022). Plants were extracted from nylon pouches with rhizosheaths intact, then briefly dipped in water to collect exudates. Exudate solutions were concentrated by freeze-drying before LC-MS/MS. Exudate metabolites were identified by comparing LC-MS/MS chromatograms and retention times to commercial standards and synthesised compounds (Table S1), with definitive ID based on matching MS^2 spectra to authentic standards.

Fig. 2 Physiological responses of white lupin to inhibitors, arsenic, and co-treatments. (A) Representative photographs of whole plants at harvest for each treatment. **(B)** Stomatal conductance (g_s) 27 and 28 days after planting (24 h and 48 h after As addition) and shoot and root fresh weight (FW) biomass at harvest. Data show means ± SE (n=5). Different letters indicate significant differences between treatments (ANOVA, Tukey HSD test, $P < 0.05$).

Fig. 3 Glutathione derivatives and phytochelatins in endosphere and root exudates in response to treatment. **(A)** Base peak chromatogram of glutathione (GSH) and phytochelatin (PC) standards (yellow) and extracted ion chromatograms of GSH (*m/z*: 308.09107; $[M+H]^+$), oxidised glutathione (GSSG) (*m/z*: 613.15862; $[M+H]^+$) and PC_2 (*m/z*: 540.14152; $[M+H]^+$), oxidised phytochelatin 2 ($oxPC_2$) (*m/z*: 538.12685; $[M+H]^+$), $oxPC_3$ and its isomer (iso-$oxPC_3$) (*m/z*: 770.17546; $[M+H]^+$) detected in endosphere (blue) and exudates (red) of As-treated lupin plants, with definitive ID based on matching retention time and MS^2 spectra. **(B)** GSH derivatives and PC abundance (Log2 peak area) in endosphere (root extracts) from controls and treated plants. **(C)** GSH derivatives and PC abundance in exudates from controls and treated plants. For all boxplots the bottom and top of the boxes correspond to the lower and upper quartiles and the center line marks the median (n = 5). Different letters indicate significant differences between treatments (ANOVA, Tukey HSD test, $P < 0.05$). Full factorial plots including all six treatments are presented in Supplementary Fig. S1. MS1 and MS2 spectra for each compound are presented in Supplementary Fig. S2. Abbreviations: As: arsenic; BSO: L-buthionine sulfoximine; N.D.: not detected.

Fig. 4 Arsenic-phytochelatin complexes in endosphere and root exudates in response to treatments. **(A)** Base peak chromatogram of synthesised arsenic-phytochelatin complex (As-PC) standards (yellow) and extracted ion chromatograms of glutathione-arsenic-phytochelatin 2 complex (GS-As-PC_2) (m/z: 460.06593; $[M+2H]^{2+}$), and arsenic-phytochelatin 3 complex (As-PC_3) (m/z: 844.09144; $[M+H]^+$) detected in endosphere (blue) and exudates (red) of arsenic-treated lupin plants, with definitive ID based on matching retention time and MS^2 spectra (Fig. S2). **(B)** Proposed structures of As-PCs in arsenic-treated lupin, adapted from Schmied-Tobies et al. (2014). 3D models generated using MolView (https://molview.org/). **(C)** Abundance (Log2 peak area) of As-PCs in root endosphere from control and treated plants. **(D)** As-PC abundance in exudates from control and treated plants. For all boxplots the bottom and top of the boxes correspond to the lower and upper quartiles and the centre line marks the median (n = 5). Different letters indicate significant differences between treatments (ANOVA, Tukey HSD

test; Kruskal-Wallis, Dunn's test; p.adj < 0.05). Full factorial plots including all six treatments are presented in Supplementary Fig. S3. MS1 and MS2 spectra for each compound are presented in Supplementary Fig. S4. Abbreviations: As: arsenic; BSO: L-buthionine sulfoximine.

Fig. 5 Arsenic treated Lupinus albus plants after chemical inhibition and corresponding putative detoxification models. Adapted from Li et al. (2016). Arrows indicate demonstrated or putative arsenic metabolic and transport pathways, while question marks highlight knowledge gaps. For all boxplots the bottom and top of the boxes correspond to the lower and upper quartiles and the centre line marks the median (n = 5); asterisks denote significant differences (P<0.05; T-test or Mann-Whitney U test). The three plant images are enlarged duplications from Figure 2A, provided as context to data here. Abbreviations: As: arsenic; BSO: L-buthionine sulfoximine; ABC: ATP-binding cassette transporter; AR: arsenate reductase; GSSG: glutathione disulfide; GSH: glutathione; PC: phytochelatins.

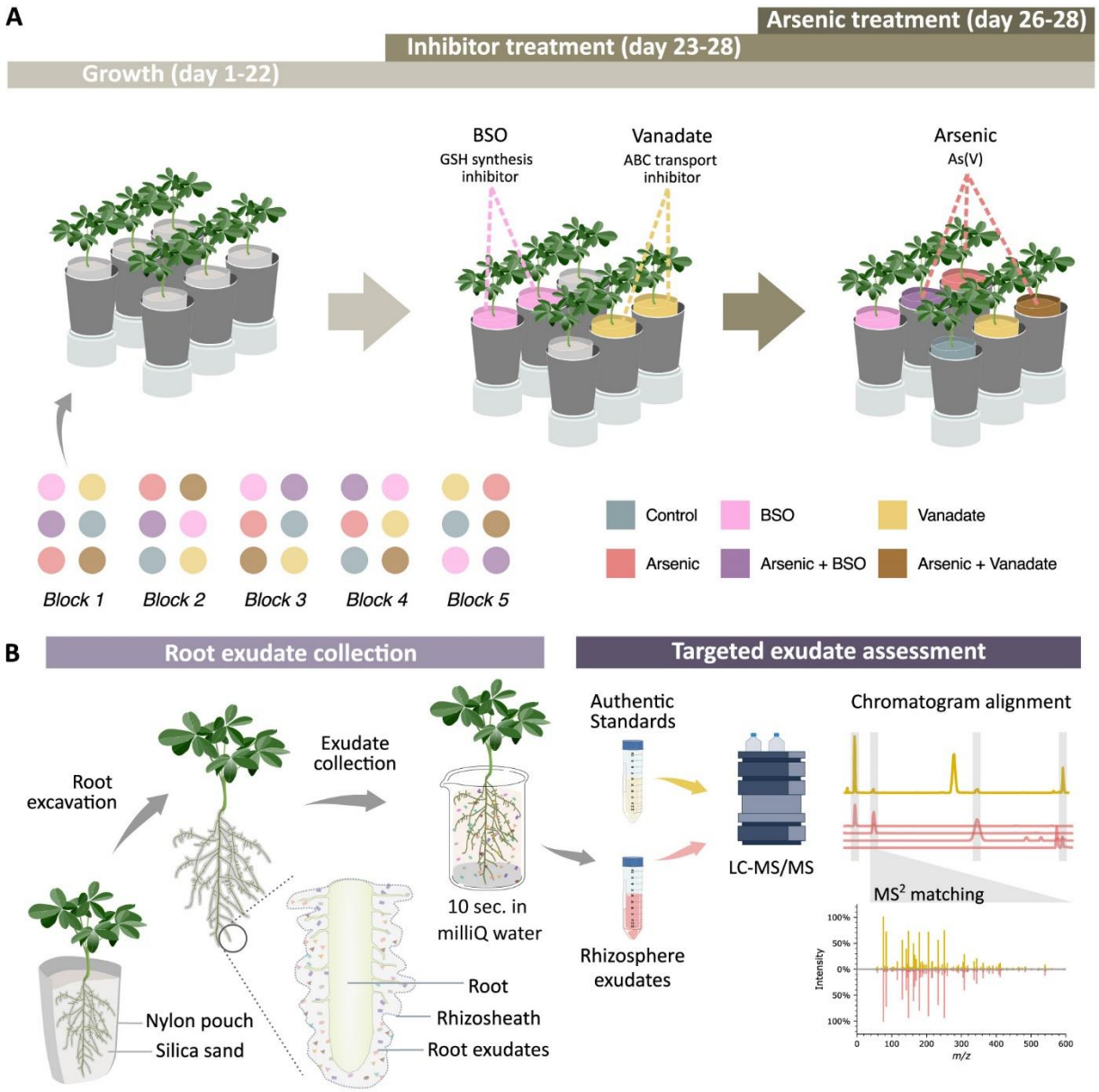

Fig. 1 Experimental design and workflow for collecting and analysing root exudates . **(A)** Experimental design (n = 5, illustrated; total plants = 30), with each plant grown for 22 days before inhibitors, arsenic, and co -treatments. **(B)** Exudate capture workflow, adapted from Frémont et al. (2022). Plants were extracted from nylon pouches with rhizosheaths intact, then briefly dipped in water to collect exudates. Exudate solutions were concentrated by freeze -drying before LC-MS/MS. Exudate metabolites were identified by comparing LC -MS/MS chromatograms and retention times to commercial standards and synthesised compounds (Table S1), with definitive ID based on matching MS ^{2} spectra to authentic standards

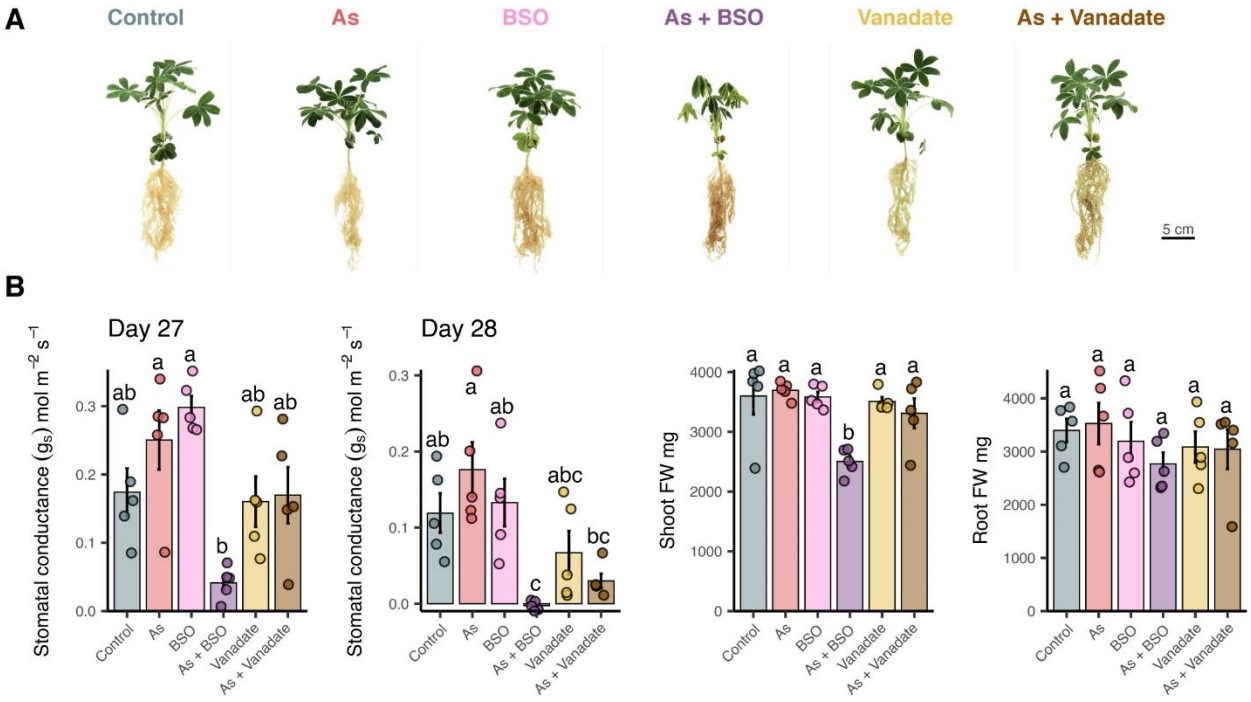

Fig. 2 Physiological responses of white lupin to inhibitors, As, and co-treatments. (A) Representative photographs of whole plants at harvest for each treatment. **(B)** Stomatal conductance (g_s) 27 and 28 days after planting (24 h and 48 h after As addition) and shoot and root fresh weight (FW) biomass at harvest. Data show means ± SE (n=5). Different letters indicate significant differences between treatments (ANOVA, Tukey HSD test, $P < 0.05$).
Abbreviations: As : arsenic; BSO: L-buthionine sulfoximine

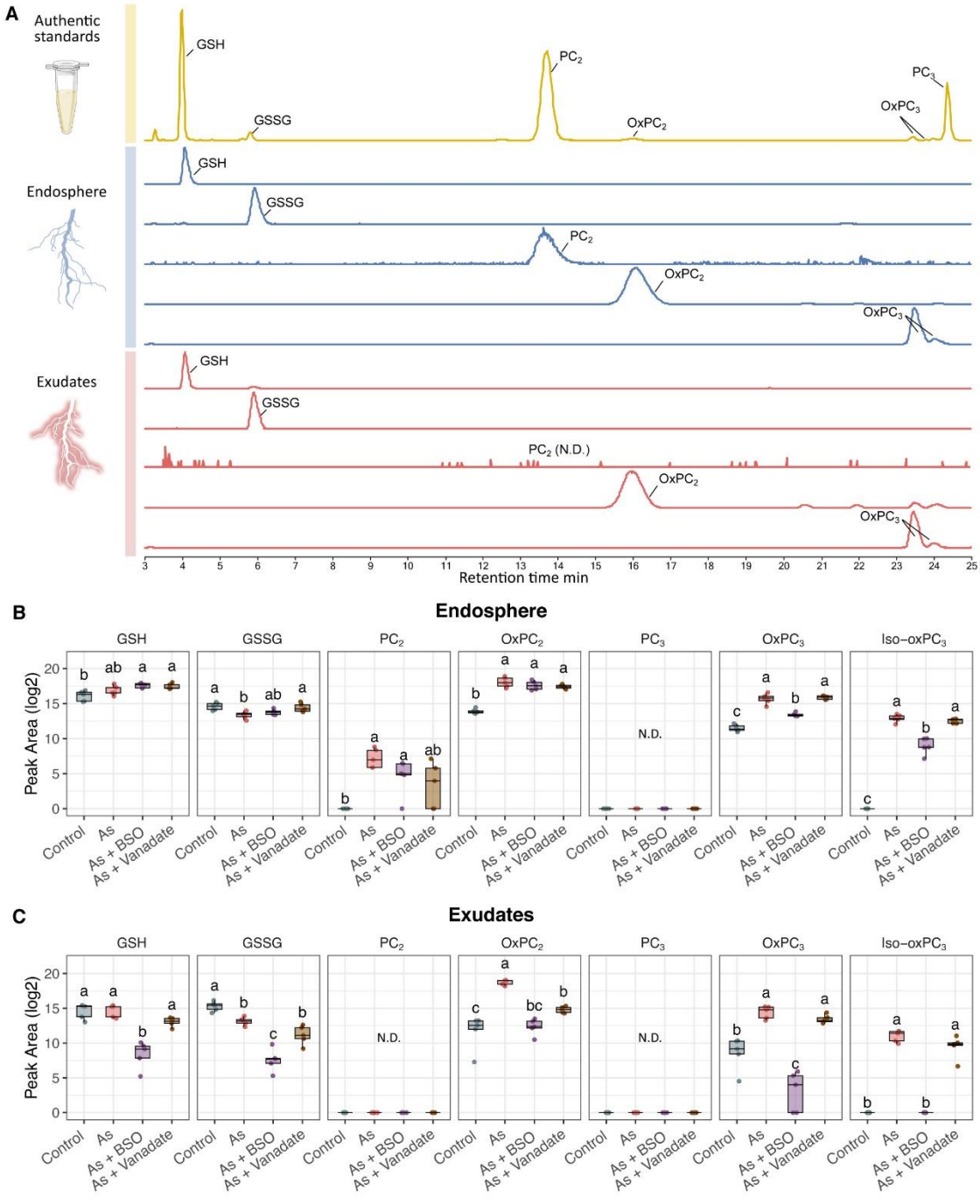

Fig. 3 Glutathione derivatives and phytochelatins in endosphere and root exudates in response to treatment. (A) Base peak chromatogram of glutathione (GSH) and phytochelatin (PC) standards (yellow) and extracted ion chromatograms of GSH (*m/z*: 308.09107; [M+H]+), oxidised glutathione (GSSG) (m/z: 613.15862; [M+H]+) and PC2 (m/z: 540.14152; [M+H]+), oxidised phytochelatin 2 (oxPC2) (m/z: 538.12685; [M+H]+), oxPC3 and its isomer (iso-oxPC3) (m/z: 770.17546; [M+H]+) detected in endosphere (blue) and exudates (red) of As-treated lupin plants, with definitive ID based on matching retention time and MS2 spectra. **(B)** GSH derivatives and PC abundance (Log2 peak area) in endosphere (root extracts) from controls and treated plants. **(C)** GSH derivatives and PC abundance in exudates from controls and treated plants. For all boxplots the bottom and top of the boxes correspond to the lower and upper quartiles and the center line marks the median (n = 5). Different letters indicate significant differences between treatments (ANOVA, Tukey HSD test, $P < 0.05$). Full factorial plots including all six treatments are presented in Supplementary Fig. S1. MS1 and MS2 spectra for each compound are presented in Supplementary Fig. S2. Abbreviations: As : arsenic; BSO: L-buthionine sulfoximine; N.D.: not detected.

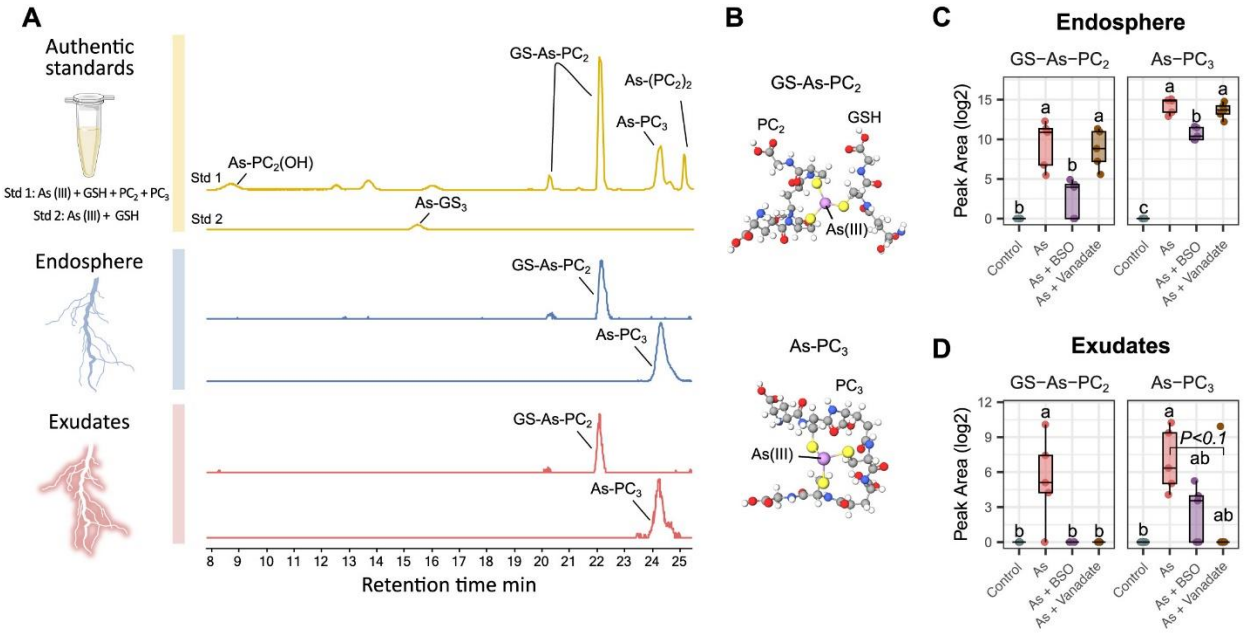

Fig. 4 Arsenic-phytochelatin complexes in endosphere and root exudates in response to treatments. (A) Base peak chromatogram of synthesised arsenic-phytochelatin complex (As-PC) standards (yellow) and extracted ion chromatograms of glutathione-arsenic-phytochelatin 2 complex (GS-As-PC2) (m/z: 460.06593; [M+2H]2+), and arsenic-phytochelatin 3 complex (As-PC3) (m/z: 844.09144; [M+H]+) detected in endosphere (blue) and exudates (red) of arsenic-treated lupin plants, with definitive ID based on matching retention time and MS2 spectra (Fig. S2). **(B)** Proposed structures of As-PCs in arsenic-treated lupin, adapted from Schmied-Tobies et al. (2014). 3D models generated using MolView (https://molview.org/). **(C)** Abundance (Log2 peak area) of As-PCs in root endosphere from control and treated plants. (D) As-PC abundance in exudates from control and treated plants. For all boxplots the bottom and top of the boxes correspond to the lower and upper quartiles and the centre line marks the median (n = 5). Different letters indicate significant differences between treatments (ANOVA, Tukey HSD test; Kruskal-Wallis, Dunn's test; p.adj < 0.05). Full factorial plots including all six treatments are presented in Supplementary Fig. S3. MS1 and MS2 spectra for each compound are presented in Supplementary Fig. S4. Abbreviations: As: arsenic; BSO: L-buthionine sulfoximine.

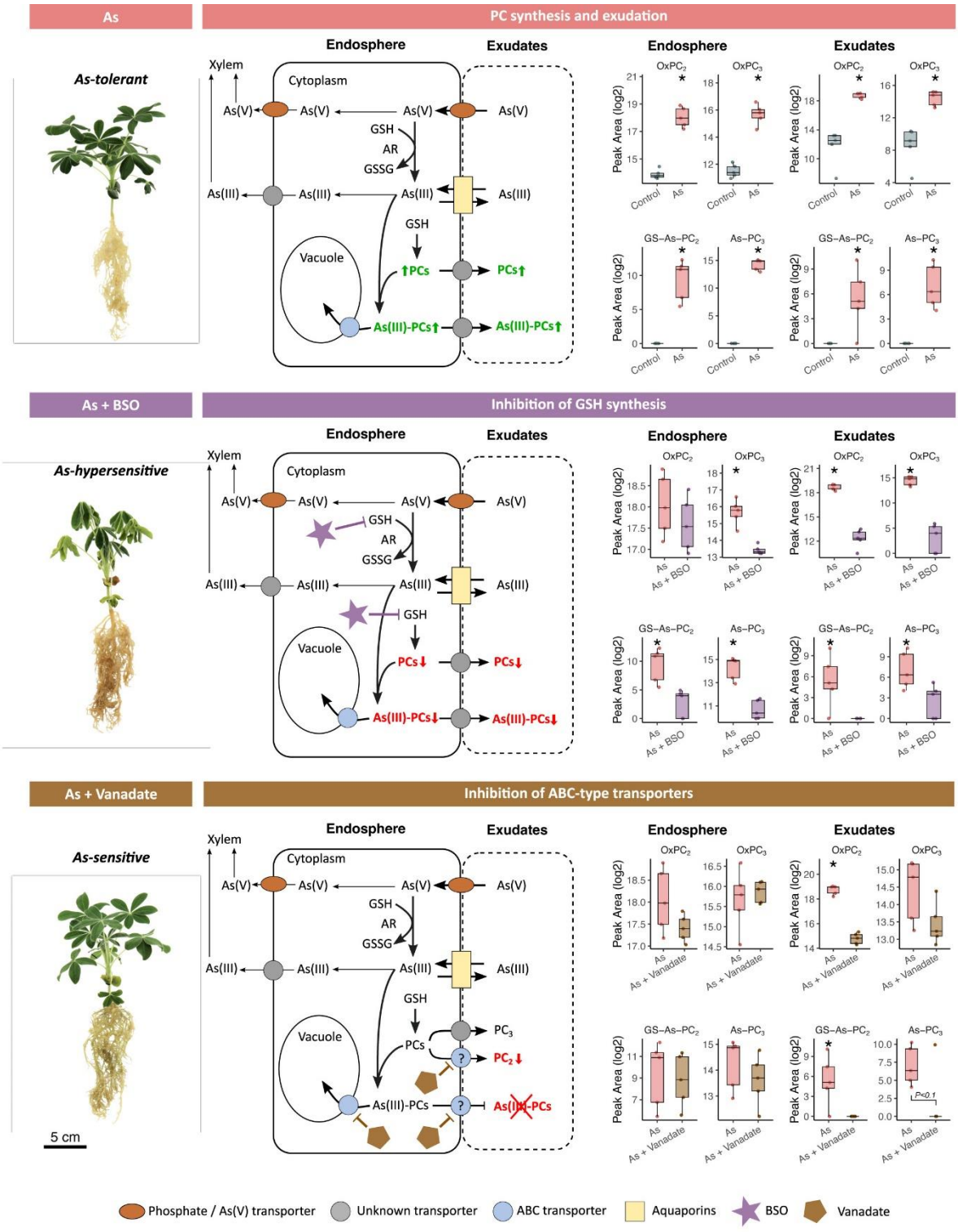

Fig. 5 Arsenic treated Lupinus albus plants after chemical inhibition and corresponding putative detoxification models. Adapted from Li et al. (2016). Arrows indicate demonstrated or putative arsenic metabolic and transport pathways, while question marks highlight knowledge gaps. For all boxplots the bottom and top of the boxes correspond to the lower and upper quartiles and the centre line marks the median (n = 5); asterisks denote significant differences (P<0.05; T-test or Mann-Whitney U test). The three plant images are enlarged duplications from Figure 2A, provided as context to data here. Abbreviations: As: arsenic; BSO: L-buthionine sulfoximine; ABC: ATP binding cassette transporter; AR: arsenate reductase; GSSG: glutathione disulfide; GSH: glutathione; PC: phytochelatins.